

Enhanced CO response of NASICON-based gas sensors using oxide-added Pt sensing electrode at low temperature operation

Taro UEDA,\* Hirotaka TAKEDA, Kai KAMADA, Takeo HYODO, and Yasuhiro SHIMIZU

Graduate School of Engineering, Nagasaki University

1-14 Bunkyo-machi, Nagasaki 852-8521, Japan

\*Corresponding author:

Taro Ueda, Dr.

Graduate School of Engineering, Nagasaki University

1-14 Bunkyo-machi, Nagasaki 852-8521, Japan

Tel: +81-95-819-2645

Fax: +81-95-819-2643

E-mail: taroueda@nagasaki-u.ac.jp

## **Abstract**

NASICON ( $\text{Na}_3\text{Zr}_2\text{Si}_2\text{PO}_{12}$ )-based solid electrolyte-type sensors equipped with various metal oxides (MO)-added Pt sensing electrode (SE, Pt( $n$ MO) ( $n$ : MO additive amount in wt%) and Pt counter electrode (CE, Pt) on the same side of the NASICON disc were fabricated and their (Pt( $n$ MO)/Pt sensors) CO-sensing properties were examined at 25–300°C. The Pt( $15\text{Bi}_2\text{O}_3$ )/Pt sensor showed the largest CO response with a change in electromotive force to a positive direction (positive response) at 25°C, while the Pt( $15\text{CeO}_2$ )/Pt sensor showed the largest negative CO response at 25°C. The CO response of the Pt( $15\text{CeO}_2$ )/Pt sensor seems to be determined by mixed potential at the triple phase boundaries (TPBs) containing the electrochemical reactions of CO oxidation and oxygen reduction. X-ray photoelectron spectroscopy of the Pt( $15\text{Bi}_2\text{O}_3$ ) SE before and after exposure to CO indicated a slight reduction of  $\text{Bi}^{3+}$  after the exposure to CO. Therefore, the additional electrochemical reactions containing the reduction of  $\text{Bi}_2\text{O}_3$  were anticipated to occur at the TPBs of the Pt( $15\text{Bi}_2\text{O}_3$ ) SE, which resulted in the large positive CO response of the Pt( $15\text{Bi}_2\text{O}_3$ )/Pt sensor. Furthermore, the addition of 15 wt%  $\text{CeO}_2$  to Pt CE of the Pt( $15\text{Bi}_2\text{O}_3$ )/Pt sensor largely enhanced the magnitude of CO response and attained relatively excellent CO selectivity against  $\text{H}_2$ .

**Keywords:** CO sensor, NASICON, Solid electrolyte,  $\text{Bi}_2\text{O}_3$

## 1. Introduction

Carbon monoxide (CO) has a great affinity for hemoglobin, which brings a critical damage to the human body by producing a reduction in cellular respiration. For example, even the small amount of CO (500 ppm) causes various symptoms such as headache, dizziness and nausea, and an increase in the CO concentration more than 1500 ppm possibly results in death for almost animate beings. CO is easily generated by imperfect combustion of fossil fuel, but we cannot recognize CO by ourselves, because it is colorless and scentless. Therefore, there is a strong demand for highly sensitive and selective CO sensors.<sup>1</sup> Some companies have so far developed and put various kinds of CO sensors, such as electrochemical, semiconducting-type and combustion-type sensors, on the market. However, electrochemical sensors use liquid or an ion-conducting polymer as an electrolyte, which makes it difficult to improve their long-term stabilities and to miniaturize these sensor packages. Other sensors have disadvantages of lack of selectivity or poor detection limits, though they show advantage of rather high stability and miniaturization. Therefore, different kinds of sensors, such as diode-type sensors and solid electrolyte-type sensors, have been examined and reported.<sup>2-6</sup> Especially, solid electrolyte-type sensors using metal oxides as a sensing electrode exhibited highly selective and sensitive responses to CO.<sup>7,8</sup> However, they use yttria-stabilized zirconia (YSZ) as an electrolyte, and hence higher operation temperature more than 450°C is required to enhance oxide-ion diffusivity in YSZ. On the other hand, we have recently reported that the sensor using NASICON (sodium super ionic conductor,  $\text{Na}_3\text{Zr}_2\text{Si}_2\text{PO}_{12}$ ) as an electrolyte and a  $\text{Bi}_2\text{O}_3$ -added Pt sensing electrode (SE) showed large response to CO at room temperature (RT) and the magnitude of CO response increased with an increase in the additive amount of  $\text{Bi}_2\text{O}_3$  in the SE.<sup>9</sup>

In this study, our efforts have been directed to the enhancement of the CO response of the

NASICON-based solid electrolyte-type sensor by adding one of various kinds of metal oxides (MO:  $\text{Al}_2\text{O}_3$ ,  $\text{Bi}_2\text{O}_3$ ,  $\text{CeO}_2$ ,  $\text{In}_2\text{O}_3$ ,  $\text{La}_2\text{O}_3$ ,  $\text{Ta}_2\text{O}_5$ ,  $\text{V}_2\text{O}_5$  and  $\text{WO}_3$ ) to the Pt SE. In addition, we have attempted to enhance the CO-sensing properties of the sensor by the addition of an appropriate MO into the Pt counter electrode (CE). We have also proposed the possible CO-sensing mechanism of representative sensors.

## 2. Experimental

### 2.1. Preparation of NASICON and MO powders

NASICON powder was synthesized from  $\text{Si}(\text{OC}_2\text{H}_5)_4$ ,  $\text{Zr}(\text{OC}_4\text{H}_9)_4$ ,  $\text{PO}(\text{OC}_4\text{H}_9)_3$  and  $\text{NaOC}_2\text{H}_5$  by a conventional sol-gel process.<sup>9-12</sup> Stoichiometric amounts of these raw materials were dissolved in pure water, together with an appropriate amount of citric acid. The mixture was subjected to heat treatment at  $80^\circ\text{C}$  to prepare an organic metal complex, followed by an overnight drying at  $120^\circ\text{C}$ . Then, the resultant solid was pyrolyzed at  $750^\circ\text{C}$  for 5 h. The powder obtained was pressed into a disc (10 mm in diameter and about 1.0 mm thick), and the disc was sintered at  $1100^\circ\text{C}$  for 5 h in air.  $\text{Bi}_2\text{O}_3$  powder was synthesized as follows.<sup>9</sup> After  $\text{Bi}(\text{NO}_3)_3 \cdot 5\text{H}_2\text{O}$  was fully dissolved in  $\text{HNO}_3$  aqueous solution, an appropriate amount of polyvinyl pyrrolidone was added to the solution as a stabilizing agent and then they were stirred for 15 min. The resultant solution was slowly and continuously dropped into  $\text{NaOH}$  solution while stirring, until the pH reached 11. After further stirring for 5 min, the resultant suspension was sonicated at 28 kHz for 30 min. The precipitate was centrifuged and washed with pure water, and this procedure was repeated several times. The resultant product was dried at  $80^\circ\text{C}$  for 2 h and then annealed at  $500^\circ\text{C}$  for 2 h.  $\text{CeO}_2$  powder was synthesized, according to the procedure reported in the literature.<sup>13</sup> After  $\text{Ce}(\text{NO}_3)_3 \cdot 6\text{H}_2\text{O}$  was dissolved in dehydrated ethanol, triethanolamine was added to the solution and then it was stirred for 1 h. Subsequently, the resultant slurry was hydrolyzed for 1 h after the addition of a small

amount of pure water. Then, the precipitate obtained was centrifuged and washed with dehydrated ethanol, and this procedure was repeated several times. The product was dried at 100°C for 12 h and then annealed at 700°C for 2 h. In<sub>2</sub>O<sub>3</sub> powder was synthesized by thermal decomposition of In(NO<sub>3</sub>)<sub>3</sub>·3H<sub>2</sub>O at 600°C in 1 h. WO<sub>3</sub> powder was synthesized by the precipitation method using Na<sub>2</sub>WO<sub>4</sub> aqueous solution. The precipitate obtained by the addition of HNO<sub>3</sub> solution into the Na<sub>2</sub>WO<sub>4</sub> aqueous solution was centrifuged and washed with pure water, and this procedure was repeated several times, followed by firing at 500°C in 2 h. Al<sub>2</sub>O<sub>3</sub> and V<sub>2</sub>O<sub>5</sub> powders were purchased from Wako Pure Chemical Industries, Ltd., Japan. La<sub>2</sub>O<sub>3</sub> and Ta<sub>2</sub>O<sub>5</sub> powders were purchased from Kishida Chemical Co., Ltd., Japan. Chemical state of the surface of Bi<sub>2</sub>O<sub>3</sub> and the mixture of Bi<sub>2</sub>O<sub>3</sub> and NASICON (Bi<sub>2</sub>O<sub>3</sub>-NASICON) powders was characterized by X-ray photoelectron spectroscopy using Al K $\alpha$  radiation (XPS, Kratos Analytical Ltd., ACIS-TLATRA DLD), and the binding energy was calibrated by using the C1s level (285.0 eV) from usual contamination.

## 2.2. Sensor fabrication

The schematic structure of a NASICON-based planar sensor is shown in Fig. 1. Both Pt paste (Tanaka Corp., TR-7907) mixed with MO (Al<sub>2</sub>O<sub>3</sub>, Bi<sub>2</sub>O<sub>3</sub>, CeO<sub>2</sub>, In<sub>2</sub>O<sub>3</sub>, La<sub>2</sub>O<sub>3</sub>, Ta<sub>2</sub>O<sub>5</sub>, V<sub>2</sub>O<sub>5</sub> or WO<sub>3</sub>) powder and pure Pt paste were applied on the same surface of the NASICON disc as a sensing electrode (SE) and a counter electrode (CE) by screen printing, respectively, and then they were annealed at 700°C for 30 min in air. The electrode fabricated from the Pt paste mixed with the MO powder was denoted as Pt(*n*MO) (*n*: the amount of the MO added to Pt (wt%)), and the sensor obtained was denoted as M/N (M: SE, N: CE). In some cases, the Pt(*n*MO) was also used as a CE.

## 2.3. Measurement of gas-sensing properties

Gas response of the sensors obtained was measured to CO (300 ppm), H<sub>2</sub> (300 ppm), and CO<sub>2</sub>

(300, 900 and 1500 ppm) balanced with dry air in a flow apparatus (gas-flow rate:  $100 \text{ cm}^3 \text{ min}^{-1}$ ) at  $25^\circ\text{C}$ ,  $100^\circ\text{C}$  and  $300^\circ\text{C}$ . The electromotive force ( $E$ , mV) of the sensors was measured with a digital electrometer as a sensing signal. The magnitude of response was defined as a difference in  $E$  between in a sample gas and in base air ( $\Delta E_{\text{Gas}}$ , Gas: CO or  $\text{H}_2$ ). The CO selectivity against  $\text{H}_2$  was defined as a ratio of CO response to  $\text{H}_2$  response ( $\Delta E_{\text{CO}}/\Delta E_{\text{H}_2}$ ).

### 3. Results and discussion

#### 3.1 CO-sensing properties of Pt(*n*MO)/Pt sensors

Typical response transients of the Pt(*n*MO)/Pt sensors (*n*: 1 or 15, MO: Bi<sub>2</sub>O<sub>3</sub>, CeO<sub>2</sub>) sensors to 300 ppm CO at 25°C are depicted in Fig. 2. Both the Pt(1Bi<sub>2</sub>O<sub>3</sub>)/Pt and Pt(15Bi<sub>2</sub>O<sub>3</sub>)/Pt sensors showed large positive CO responses. In addition, the *E* values of Pt(*n*Bi<sub>2</sub>O<sub>3</sub>)/Pt sensors in air positively shifted with an increase in the additive amount of Bi<sub>2</sub>O<sub>3</sub>, but the magnitude of CO response ( $\Delta E_{\text{CO}}$ ) of the Pt(15Bi<sub>2</sub>O<sub>3</sub>)/Pt sensor was comparable with that of the Pt(1Bi<sub>2</sub>O<sub>3</sub>)/Pt sensor. We have shown previously that the magnitude of CO response of Pt(*n*Bi<sub>2</sub>O<sub>3</sub>)/Pt sensors decreased with a decrease in the additive amount of Bi<sub>2</sub>O<sub>3</sub> to Pt electrode “*n*” less than ca. 1 wt%, and that could reach to almost zero with a further decrease in the additive amount of Bi<sub>2</sub>O<sub>3</sub>.<sup>9</sup> In addition, we also reported that the Pt(1Bi<sub>2</sub>O<sub>3</sub>)/Pt sensor showed an almost linear relationship between the CO response and the logarithm of CO concentration (1–3000 ppm) at 25°C and a clear response even to 1 ppm CO at 25°C (ca. 17 mV).<sup>9</sup> This result demonstrated that even the addition of 1 wt% Bi<sub>2</sub>O<sub>3</sub> into the Pt SE was quite effective in improving the CO-sensing properties. However, the *E* values in air of these Pt(*n*Bi<sub>2</sub>O<sub>3</sub>)/Pt sensors shifted to the negative direction after the 1st CO exposure, even though the *E* value of the Pt(*n*Bi<sub>2</sub>O<sub>3</sub>)/Pt sensors at the the 1st CO exposure was comparable to that at the 2nd CO exposure. Therefore, the 2nd CO responses of these sensors were slightly larger than their 1st CO responses. In addition, the behavior of the subsequent responses of the Pt(*n*Bi<sub>2</sub>O<sub>3</sub>)/Pt sensors to CO in air was quite comparable to that of their 2nd CO responses.<sup>9</sup>

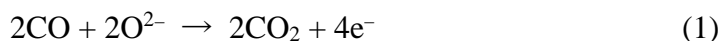
On the other hand, the Pt(*n*CeO<sub>2</sub>)/Pt sensors showed negative responses to CO. The *E* values of Pt(*n*CeO<sub>2</sub>)/Pt sensors in air also positively shifted with an increase in the additive amount of CeO<sub>2</sub>, and those in CO balanced with air was negatively shifted with an increase in the additive amount of CeO<sub>2</sub>. As a result, the  $\Delta E_{\text{CO}}$  of the Pt(*n*CeO<sub>2</sub>)/Pt sensors increased with an increase in the additive amount of CeO<sub>2</sub>. The response behavior of the Pt(*n*CeO<sub>2</sub>)/Pt sensors was relatively stable with the

fast response speeds (especially in the case of the Pt( $15\text{CeO}_2$ )/Pt sensor), whereas the recovery behavior of Pt( $n\text{CeO}_2$ )/Pt sensors was rather unstable as shown in Fig. 2(b). Namely, the large overshoot behavior of  $E$  was observed, as soon as 300 ppm CO was removed from the atmosphere. In addition, the exposure of these sensors to CO induced a shift in their  $E$  values to a negative direction by repetition of the CO exposure, and thus the CO responses of Pt( $n\text{CeO}_2$ )/Pt sensors slightly increased with an increase in the number of CO exposure.

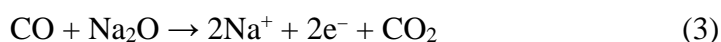
Figure 3 shows variations in 2nd CO responses of Pt( $15\text{MO}$ )/Pt sensors with operating temperature. The Pt( $15\text{Bi}_2\text{O}_3$ )/Pt sensor showed the largest positive CO response at 25°C among all the sensors, while the Pt( $15\text{CeO}_2$ )/Pt sensor showed the largest negative CO response at 25°C. The CO response of Pt( $15\text{Bi}_2\text{O}_3$ )/Pt sensor decreased with an increase in the operating temperature, as reported previously.<sup>9</sup> On the contrary, the magnitude of CO response of most sensors, except for Pt( $15\text{Bi}_2\text{O}_3$ )/Pt and Pt( $15\text{La}_2\text{O}_3$ )/Pt sensors, tended to shift positively with an increase in the operating temperature. Among these sensors, the Pt( $15\text{Al}_2\text{O}_3$ )/Pt only showed negative CO response at 100°C. On the other hand, CO response of the Pt( $15\text{La}_2\text{O}_3$ )/Pt sensor was less dependent on the operating temperature. All sensors showed positive CO responses at 300°C, and the CO response of the Pt( $15\text{Bi}_2\text{O}_3$ )/Pt sensor was the largest among them.

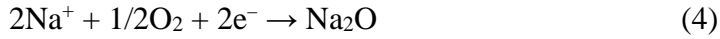
### 3.2 CO-sensing mechanism of Pt( $15\text{Bi}_2\text{O}_3$ )/Pt and Pt( $15\text{CeO}_2$ )/Pt sensors at 25°C

Generally, yttria-stabilized zirconia (YSZ)-based sensors showed negative CO response in air at elevated temperatures and the SE potential is considered to be determined on the basis of mixed-potential theory involving the electrochemical CO oxidation (eq. (1)) and  $\text{O}_2$  reduction (eq. (2)), which take place simultaneously at the TPBs (SE/YSZ/gas).<sup>7, 14–16</sup> This CO-sensing mechanism was proved by the estimation of current( $I$ )-voltage( $V$ ) curves of these electrochemical reactions.<sup>7, 16</sup>



We have already reported that the electrode potential of Pt attached with NASICON (CE in this study) negatively shifted at 25°C when CO was injected into air.<sup>9</sup> Therefore, it is really essential that the magnitude of negative-shifted potential of the Pt(15CeO<sub>2</sub>) SE was much larger than that of the negative-shifted potential of the Pt CE, when CO was injected into air, because the Pt(15CeO<sub>2</sub>)/Pt sensor showed the negative CO response in air at 25°C. Generally, the catalytic activity of Pt is easily degraded by the CO adsorption, especially at low temperature.<sup>17, 18</sup> However, Hong et al. recently reported that Pt-dispersed CeO<sub>2</sub>-based catalysts effectively oxidized CO, because negatively charged metallic Pt species exists on the CeO<sub>2</sub>, which could effectively promote the adsorption of oxygen.<sup>18</sup> In addition, it is well known that the valence of Ce in CeO<sub>2</sub> easily change between 3+ and 4+, and thus CeO<sub>2</sub> has an oxygen storage property.<sup>19</sup> For example, Satsuma et al. reported that Pd-loaded CeO<sub>2</sub> showed the largest CO oxidation activity at low temperature among various Pd-loaded metal oxides, by temperature-programmed reduction conducted by using CO. Namely, they showed that CO was easily oxidized to CO<sub>2</sub> even at RT and the first reduction peak was observed at 106°C, which verified the oxygen supply for CO oxidation at low temperature.<sup>20</sup> These results support that the addition of CeO<sub>2</sub> into the Pt electrode can enhance the electrochemical CO oxidation, and thus the potential of the Pt(15CeO<sub>2</sub>) SE is also considered to be determined on the basis of mixed-potential theory. Presently, we believe that the electrode potential of both the SE and the CE was determined by the following electrochemical reactions, and the addition of CeO<sub>2</sub> into the Pt electrode largely reduced the overpotential of the electrochemical CO oxidation, which resulted in quite low electrode potential of the Pt(15CeO<sub>2</sub>) SE in CO balanced with air (namely, largely negative CO response) of the Pt(15CeO<sub>2</sub>)/Pt sensor.<sup>21</sup>





On the other hand, the Pt(*15*Bi<sub>2</sub>O<sub>3</sub>)/Pt sensor showed a large positive *E* value in CO balanced with air. We have observed the intermediate layer at the interface between the Pt(*15*Bi<sub>2</sub>O<sub>3</sub>) SE and NASICON by the cross-sectional SEM view of the Pt(*15*Bi<sub>2</sub>O<sub>3</sub>)/Pt sensor. In addition, XRD analysis of the mixture of Bi<sub>2</sub>O<sub>3</sub> and NASICON, which was annealed at 700°C for 30 min, showed the existence of both BiPO<sub>4</sub> and Bi<sub>2</sub>SiO<sub>5</sub> phases in the intermediate layer.<sup>9</sup> On the other hand, any intermediate layers were not observed at the interface between the Pt(*15*CeO<sub>2</sub>) SE and NASICON of the Pt(*15*CeO<sub>2</sub>)/Pt sensor (not shown here), which showed large negative CO response. Therefore, it is likely that Bi-based intermediate materials at the interface between Pt(*15*Bi<sub>2</sub>O<sub>3</sub>) SE and NASICON largely contributed to the large positive response of the Pt(*15*Bi<sub>2</sub>O<sub>3</sub>)/Pt sensor. In order to clarify effects of the intermediate materials on the CO-sensing properties, the chemical state of the surface of Bi<sub>2</sub>O<sub>3</sub> and the mixture of Bi<sub>2</sub>O<sub>3</sub> and NASICON (Bi<sub>2</sub>O<sub>3</sub>-NASICON, annealed at 700°C for 30 min) before and after the exposure to CO was estimated by XPS. Figure 4 shows XPS spectra of Bi4f of Bi<sub>2</sub>O<sub>3</sub> and Bi<sub>2</sub>O<sub>3</sub>-NASICON powders before and after exposure to 3000 ppm CO balanced with air at 700°C for 2 h. Two peaks corresponding to Bi4f<sub>5/2</sub> (e.g., ca. 164.1 eV and ca. 164.5 eV for Bi<sub>2</sub>O<sub>3</sub> and Bi<sub>2</sub>O<sub>3</sub>-NASICON, respectively, before the exposure to CO) and Bi4f<sub>7/2</sub> (e.g., ca. 158.8 eV and ca. 159.2 eV for Bi<sub>2</sub>O<sub>3</sub> and Bi<sub>2</sub>O<sub>3</sub>-NASICON, respectively, before the exposure to CO) were observed, and all the Bi4f peaks indicate the chemical state of Bi<sup>3+</sup>.<sup>22-24</sup> In addition, the binding energies of Bi4f of Bi<sub>2</sub>O<sub>3</sub>-NASICON was higher than those of Bi<sub>2</sub>O<sub>3</sub>, because BiPO<sub>4</sub> and Bi<sub>2</sub>SiO<sub>5</sub> produced in the Bi<sub>2</sub>O<sub>3</sub>-NASICON after annealed at 700°C for 30 min<sup>9</sup> and the binding energies of Bi4f in BiPO<sub>4</sub> and Bi<sub>2</sub>SiO<sub>5</sub> are higher than those of Bi<sub>2</sub>O<sub>3</sub>.<sup>25-27</sup> For example, the binding energies of Bi4f<sub>7/2</sub> for BiPO<sub>4</sub> and Bi<sub>2</sub>SiO<sub>5</sub> were ca. 159.5 eV and ca. 160.8 eV, respectively,<sup>25, 27</sup> while the binding energy of Bi4f<sub>7/2</sub> for Bi<sub>2</sub>O<sub>3</sub> was ca. 158.6 eV.<sup>22</sup> These binding energies slightly decreased after the exposure to CO. The binding energies of Bi4f<sub>5/2</sub> were ca. 163.9 eV and ca. 164.4

eV for Bi<sub>2</sub>O<sub>3</sub> and Bi<sub>2</sub>O<sub>3</sub>-NASICON, respectively, and that of Bi4f<sub>7/2</sub> were ca. 158.6 eV and ca. 159.1 eV for Bi<sub>2</sub>O<sub>3</sub> and Bi<sub>2</sub>O<sub>3</sub>-NASICON, respectively, after the exposure to CO. This is mainly due to a decrease in the amount of oxygen species (e.g., oxygen adsorbates and lattice oxygen) and slight reduction in the Bi<sup>3+</sup> species on the surface of Bi<sub>2</sub>O<sub>3</sub> and Bi<sub>2</sub>O<sub>3</sub>-NASICON, upon exposure to CO. Grzybowska et al. have reported that the heat treatment of Bi<sub>2</sub>Mo<sub>2</sub>O<sub>9</sub> at 470°C in H<sub>2</sub> atmosphere slightly decreased the binding energy of Bi4f<sub>7/2</sub> from 159.7 eV to 159.1 eV.<sup>28</sup> Farin et al. has also shown that the binding energy of Bi4f<sub>7/2</sub> of Bi<sub>2</sub>Mo<sub>2</sub>O<sub>9</sub> was decreased by the oxidation of propene over Bi<sub>2</sub>Mo<sub>2</sub>O<sub>9</sub> in air.<sup>29</sup> These studies strongly support that the slight decrease in the binding energies of Bi4f<sub>7/2</sub> of Bi<sub>2</sub>O<sub>3</sub> and Bi<sub>2</sub>O<sub>3</sub>-NASICON after exposure to CO indicates the slight reduction of Bi-species at their surface.

On the basis of these results and discussion, we have firstly clarified the role in the Bi-species in the intermediate layer at the interface between the Pt(*15*Bi<sub>2</sub>O<sub>3</sub>) SE and NASICON for the large positive CO of the Pt(*15*Bi<sub>2</sub>O<sub>3</sub>)/Pt sensor. Considering the easy reduction of Bi-species upon exposure to CO, the electrode potential of the Pt(*15*Bi<sub>2</sub>O<sub>3</sub>) SE is dominated by the balance of CO oxidation (eq. (3)) and possible reduction reactions as follows.

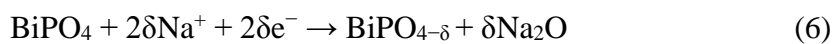
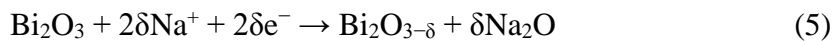


Figure 3 indicates that the *E* value of the Pt(*15*Bi<sub>2</sub>O<sub>3</sub>) SE in CO balanced with air is positively larger than those of other SEs, as all the sensors used Pt as a CE material. The fact strongly supports that the electrode potentials of these reactions are positively larger than that of oxygen redox reaction and/or the overpotential for these reactions, which is necessary for obtaining the same amount of current as electrochemical CO oxidation, is smaller than that for oxygen redox reaction.

CO<sub>2</sub> generated by the oxidation reaction of CO may contribute the response behavior of the Pt(15Bi<sub>2</sub>O<sub>3</sub>)/Pt sensor. Therefore, response transients of the Pt(15Bi<sub>2</sub>O<sub>3</sub>)/Pt sensor to various concentrations of CO<sub>2</sub> at 25°C were also investigated as shown in Fig. 5. The *E* value slightly shifted to the positive direction upon exposure to 300 ppm CO<sub>2</sub> balanced with air, and the *E* value didn't recover to the original level when CO<sub>2</sub> was removed. In addition, the magnitude of response to both 900 and 1500 ppm CO<sub>2</sub> was smaller than that of 300 ppm CO<sub>2</sub>. The fact that the response of the Pt(15Bi<sub>2</sub>O<sub>3</sub>)/Pt sensor to 300 ppm CO<sub>2</sub> (ca. 19 mV) was much smaller than that to 300 ppm CO (ca. 235 mV) indicates that the CO response does not originate from the electrochemical reaction of Bi<sub>2</sub>O<sub>3</sub>-NASICON and CO<sub>2</sub> which is produced through the CO oxidation on the electrode.

In addition, some carbonate species are possibly formed at the TPBs by the reaction of the Bi<sub>2</sub>O<sub>3</sub> and Bi<sub>2</sub>O<sub>3</sub>-NASICON with CO<sub>2</sub>, which was produced in the electrochemical CO oxidation, and they may also have some influence on the CO-sensing properties. Therefore, XPS spectra of C1s of the Bi<sub>2</sub>O<sub>3</sub> and Bi<sub>2</sub>O<sub>3</sub>-NASICON powders before and after exposure to 3000 ppm CO balanced with air at 700°C for 2 h were also examined as shown in Fig. 6. The peak at 285.0 eV is typically assigned to adventitious (aliphatic) carbon, which is adsorbed on the surface of all samples exposed to the atmosphere. Broad peaks centered at ca. 289.2 eV and ca. 288.0–289.0 eV for Bi<sub>2</sub>O<sub>3</sub> and Bi<sub>2</sub>O<sub>3</sub>-NASICON, respectively, which were derived from carbonate species<sup>30, 31</sup>, were observed before the exposure to CO. The heat treatment at 700°C seems to produce the carbonate species on their surface by the reaction with CO<sub>2</sub> in the atmospheric air. The intensity of the peak centered at 289.2 eV for Bi<sub>2</sub>O<sub>3</sub> increased by the exposure to CO, which shows that CO was oxidized even at RT and then the produced CO<sub>2</sub> reacted with Bi<sub>2</sub>O<sub>3</sub> to form bismuth carbonate such as (BiO)<sub>2</sub>CO<sub>3</sub><sup>31</sup>. On the other hand, the broad peak of Bi<sub>2</sub>O<sub>3</sub>-NASICON (centered at ca. 288.0–290.0 eV) after the exposure to CO was quite comparable to that before the exposure to CO, probably because the NASICON inhibited the production of carbonate species on the surface of the Bi<sub>2</sub>O<sub>3</sub>-NASICON.

These results indicate that the amount of carbonate species produced by the CO exposure at the TPBs of the Pt( $15\text{Bi}_2\text{O}_3$ ) SE is not so large to control the electrode potential, but this fact may explain the negative shift in the  $E$  values in air of these Pt( $n\text{Bi}_2\text{O}_3$ )/Pt sensors after the 1st CO exposure. Namely, the production of small amount of carbonate species at the TPBs slightly affects the balance of the electrochemical reactions at TPBs, which probably changes the  $E$  values in air after the 1st CO exposure. However, the amount of carbonate species produced was tiny as examined, and thus the  $E$  values in air were almost stable after the subsequent CO exposure.

### 3.3 Combination of Pt( $15\text{Bi}_2\text{O}_3$ ) and Pt( $15\text{CeO}_2$ ) electrodes to enhance CO response

The use of Pt( $15\text{Bi}_2\text{O}_3$ ) and Pt( $15\text{CeO}_2$ ) as a SE and a CE, respectively, is expected to be quite effective in enhancing the CO response at  $25^\circ\text{C}$ , as the Pt( $15\text{Bi}_2\text{O}_3$ )/Pt and Pt( $15\text{CeO}_2$ )/Pt sensors showed the largest positive and negative CO responses at  $25^\circ\text{C}$ , respectively (see Fig. 4). Therefore, the Pt( $15\text{Bi}_2\text{O}_3$ )/Pt( $15\text{CeO}_2$ ) sensor was actually fabricated, and the response transients to 300 ppm CO and 300 ppm  $\text{H}_2$  of the sensor were examined as shown in Fig. 7. The  $E$  value of the Pt( $15\text{Bi}_2\text{O}_3$ )/Pt( $15\text{CeO}_2$ ) sensor in air also largely negative-shifted upon the 1st exposure to CO, and the Pt( $15\text{Bi}_2\text{O}_3$ )/Pt( $15\text{CeO}_2$ ) sensor showed quite large CO response (ca. 391 mV) at the 2nd CO response. The magnitude of the CO response was roughly coincided with the balance of the CO responses of both Pt( $15\text{Bi}_2\text{O}_3$ )/Pt sensor (ca. 235 mV) and Pt( $15\text{CeO}_2$ )/Pt sensor (ca. -202 mV). In addition, the magnitude of response of the Pt( $15\text{Bi}_2\text{O}_3$ )/Pt( $15\text{CeO}_2$ ) sensor to 300 ppm  $\text{H}_2$  was ca. 63 mV, and thus the sensor showed rather good CO selectivity against  $\text{H}_2$ . Practical CO sensors are required to show relatively low response to other inflammable gases such as hydrocarbons and  $\text{H}_2$ , because CO is generated by the imperfect combustion of fossil fuels or hydrogen production from fossil fuels.<sup>32</sup> These results show that the Pt( $15\text{Bi}_2\text{O}_3$ )/Pt( $15\text{CeO}_2$ ) sensor is the most promising candidate for CO sensors operating at RT, in this study.

#### 4. Conclusion

CO-sensing properties of the NASICON-based solid electrolyte-type sensors using the eight kinds of MO-added Pt SEs were examined in the temperature range of 25–300°C. Among them, the magnitude of response of the Pt(*15*Bi<sub>2</sub>O<sub>3</sub>)/Pt sensor showed the largest CO response at 25°C, while the Pt(*15*CeO<sub>2</sub>)/Pt sensor showed the largest negative response at 25°C. The addition of CeO<sub>2</sub> to Pt CE of the Pt(*15*Bi<sub>2</sub>O<sub>3</sub>)/Pt sensor further enhanced the magnitude of CO response. According to the XPS analysis, the binding energies of Bi<sup>3+</sup> of the mixture of Bi<sub>2</sub>O<sub>3</sub> and NASICON were slightly reduced after the exposure to CO. Therefore, we proposed the possible reduction reactions at the triple phase boundaries, which induced the large and positive CO response on the basis of mixed-potential theory.

## References

1. C. M. Chiu and Y. H. Chang, *Mater. Sci. Eng. A-Struct. Mater. Prop. Microstruct. Process.*, **266**, 93 (1999).
2. F. Juang, Y. Fang, Y. Chiang, T. Chou, and C. Lin, *Sens. Actuators B*, **156**, 338 (2011).
3. A. Hosoya, S. Tamura, and N. Imanaka, *J. Ceram. Soc. Jpn.*, **122**, 601 (2014).
4. A. Hosoya, S. Tamura, and N. Imanaka, *Chem. Lett.*, **42**, 441 (2013).
5. V. Plashnitsa, S. Anggraini, and N. Miura, *Electrochem. Commun.*, **13**, 444 (2011).
6. S. Anggraini, V. Plashnitsa, P. Elumalai, and M. Breedon, *Sens. Actuators B*, **160**, 1273 (2011).
7. F. Yujio, V. V. Plashnitsa, M. Breedon, and N. Miura, *Langmuir*, **28**, 1638 (2012).
8. F. Sun, X. Li, L. Liu, and J. Wang, *Sens. Actuators B*, **184**, 220 (2013).
9. H. Takeda, T. Ueda, K. Kamada, K. Matsuo, T. Hyodo, and Y. Shimizu, *Electrochim. Acta*, **155**, 8 (2015).
10. T. Hyodo, T. Furuno, S. Kumazawa, Y. Shimizu, and M. Egashira, *Sens. Mater.*, **19**, 365 (2007).
11. M. Morio, T. Hyodo, Y. Shimizu, and M. Egashira, *Sens. Actuators B*, **139**, 23 (2009).
12. Y. L. Huang, A. Caneiro, M. Attari, and P. Fabry, *Thin Solid Films*, **196**, 283 (1991).
13. L. Kangqiang, Z. Mingqiang, *J. Rare Earths*, **28**, 680 (2010).
14. V. V. Plashnitsa, S. A. Anggraini, N. Miura, *Electrochem. Commun.*, **13**, 444 (2011).
15. R. Wu, C. Hu, C. Yeh, P. Su, *Sens. Actuators B*, **96**, 596 (2003).
16. S. A. Anggraini, V. V. Plashnitsa, P. Elumalai, M. Breedon, N. Miura, *Sens. Actuators B*, **160**, 1273 (2011).
17. H. Igarashi, T. Fujino, M. Watanabe, *J. Electroanal. Chem.*, **391**, 119 (1995).
18. X. Hong, Y. Sun, *Catal. Lett.*, **146**, 2001 (2016).
19. M. Ozawa, T. Okouchi, and M. Haneda, *Catal. Today*, **242**, 329 (2015).
20. A. Satsuma, K. Osaki, M. Yanagihara, J. Ohyama, K. Shimizu, *Appl. Catal. B-Environ.*, **132**,

511 (2013) .

21. L. Xishuang, Y. Shiqi, Z. Tiegang, D. Quan, Z. Han, L. Jianguo, Q. Baofu, L. Geyu, *Sens. Lett.*, **9**(2), 832 (2011).
22. S. Shamaila, A. Khan, L. Sajjad, F. Chen, and J. Zhang, *Appl. Catal. B-Environ.*, **94**, 272 (2010).
23. L. Zhang, Y. Hashimoto, T. Taishi, I. Nakamura, and Q. Ni, *Appl. Surf. Sci.*, **257**, 6577 (2011).
24. J. Li, J. Zhong, X. He, S. Huang, J. Zeng, and J. He, *Appl. Surf. Sci.*, **284**, 527 (2013).
25. A. K. R. Police, S. Basavaraju, D. K. Valluri, and S. Machiraju, *J. Mater. Sci. Technol.*, **29**, 639 (2013).
26. S. Wu, H. Zheng, Y. Wu, W. Lin, T. Xu, and M. Guan, *Ceram. Int.*, **40**, 14613 (2014).
27. Z. Li, S. Yang, J. Zhou, D. Li, X. Zhou, C. Ge, and Y. Fang, *Chem. Eng. J.*, **241**, 344 (2014).
28. B. Grzybowska, J. Haber, W. Marczewski, and L. Ungier, *J. Catal.*, **42**, 327 (1976).
29. B. Farin, A. H.A. M. Videla, S. Specchia, and E. M. Gaigneaux, *Catal. Today*, **257**, 11 (2015).
30. S. Garciaa, R.J. Rosenbauerb, J. Palandric and M.M. Maroto-Valera, *Int. J. Greenh. Gas Control*, **7**, 89 (2012).
31. F. Dong, Y. Sun, M. Fu, W.-K. Ho, S.- C. Lee, and Z. Wu, *Langmuir*, **28**, 766 (2011).
32. C. Coutaceau and S. Baranton, *Wiley Interdiscip. Rev. Energy Environ.*, **5**, 388 (2016).

### ***Figure captions***

- Fig. 1 Schematic structure of a typical NASICON-based planar gas sensor.
- Fig. 2 Response transients of (a) Pt( $n\text{Bi}_2\text{O}_3$ )/Pt sensors and (b) Pt( $n\text{CeO}_2$ )/Pt sensors ( $n$ : 1 or 15 wt%) to 300 ppm CO at 25°C.
- Fig. 3 Temperature dependence of magnitude of response to 300 ppm CO of Pt(15MO)/Pt sensors.
- Fig. 4 XPS spectra of Bi4f of (a)  $\text{Bi}_2\text{O}_3$  and (b)  $\text{Bi}_2\text{O}_3$ -NASICON powders before and after exposure to 3000 ppm CO.
- Fig. 5 Response transients of Pt(15 $\text{Bi}_2\text{O}_3$ )/Pt sensor to  $\text{CO}_2$  (300, 600, 900 ppm) at 25°C.
- Fig. 6 XPS spectra of C1s of (a)  $\text{Bi}_2\text{O}_3$  and (b)  $\text{Bi}_2\text{O}_3$ -NASICON powders before and after exposure to 3000 ppm CO.
- Fig. 7 Response transients of Pt(15 $\text{Bi}_2\text{O}_3$ )/Pt(15 $\text{CeO}_2$ )/Pt sensor to 300 ppm CO and 300 ppm  $\text{H}_2$  at 25°C.

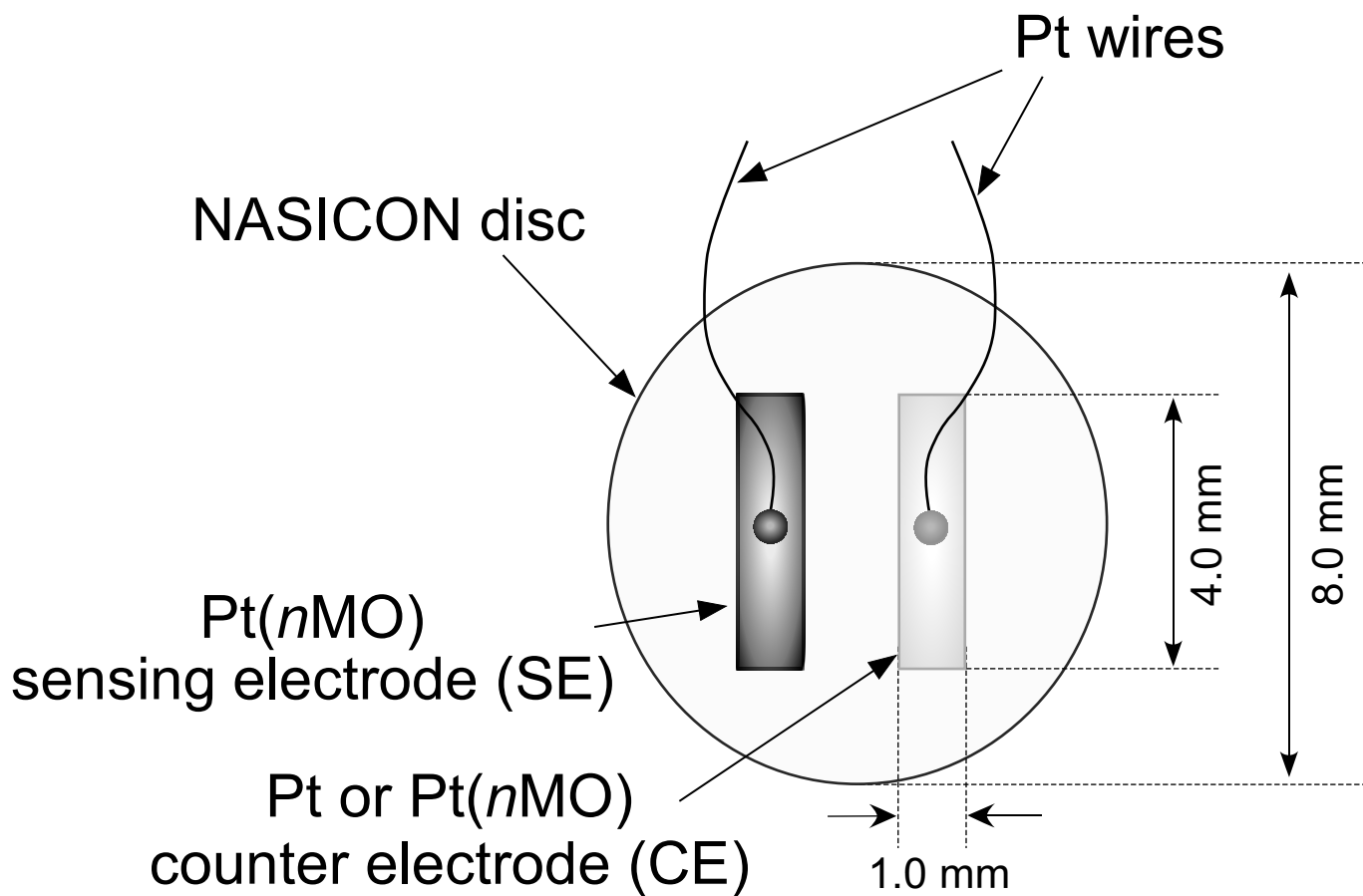


Fig.1. Ueda et al.

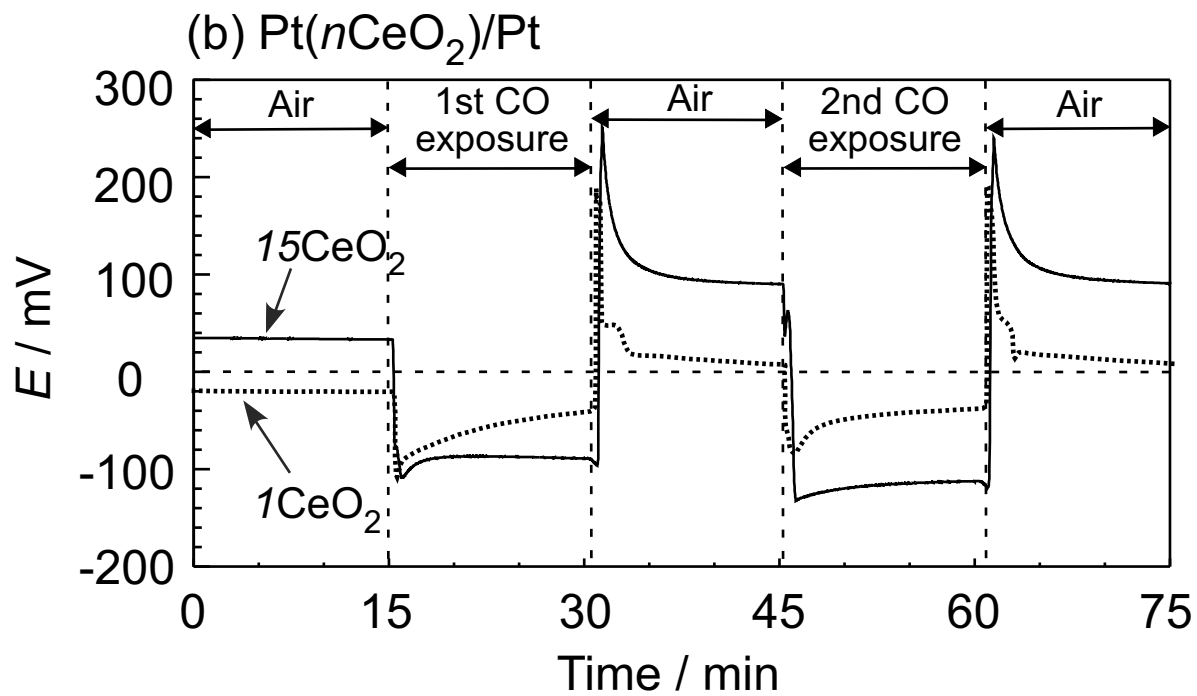
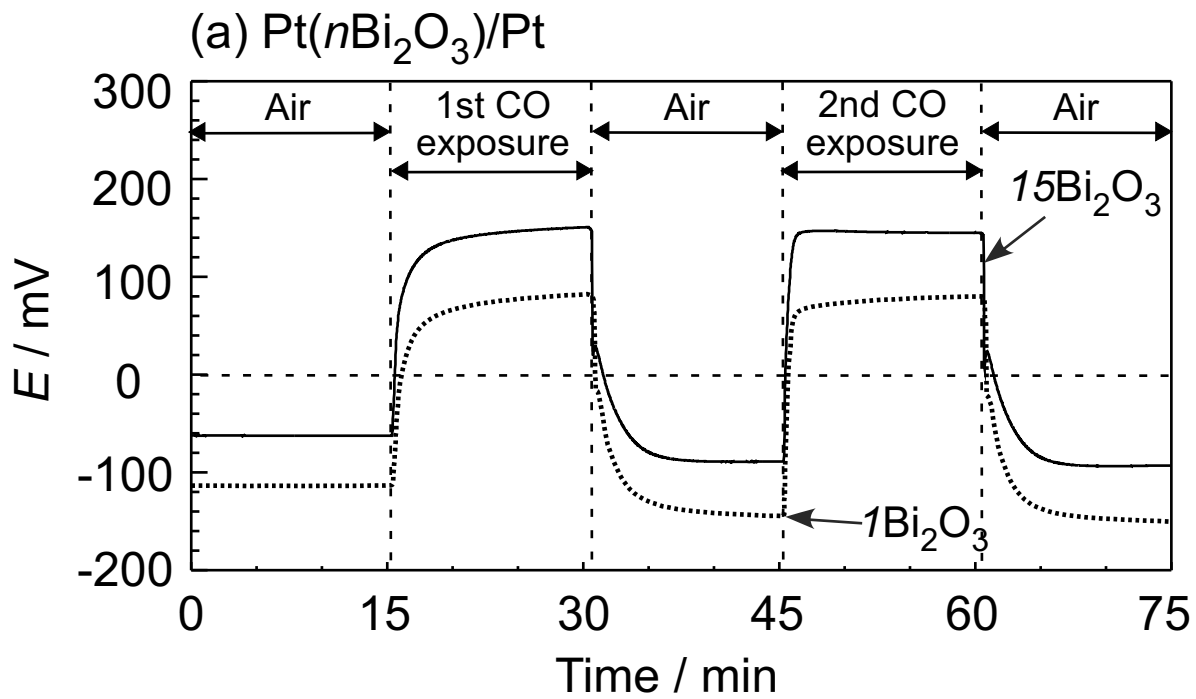


Fig. 2. Ueda et al.

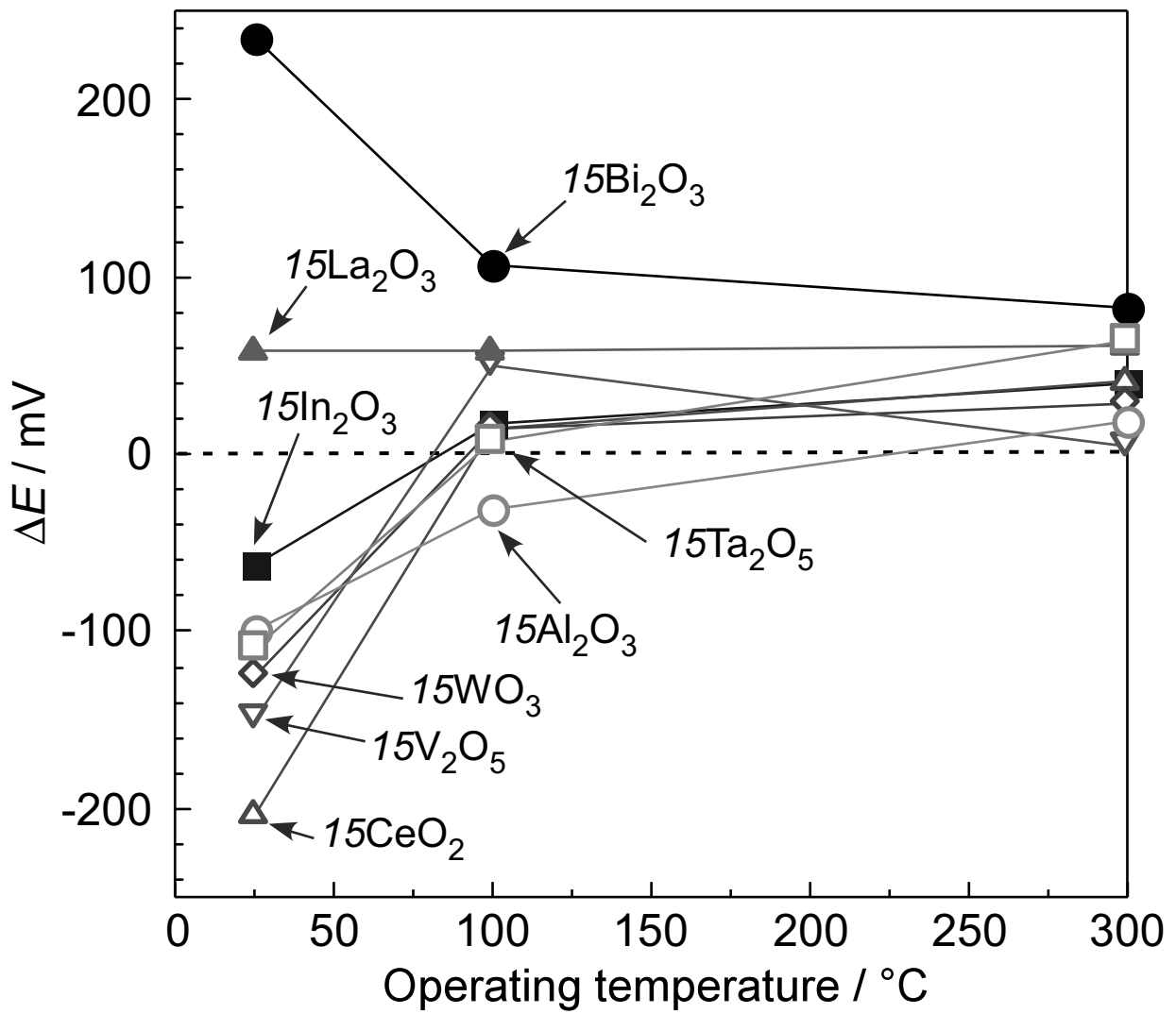


Fig. 3. Ueda et al.

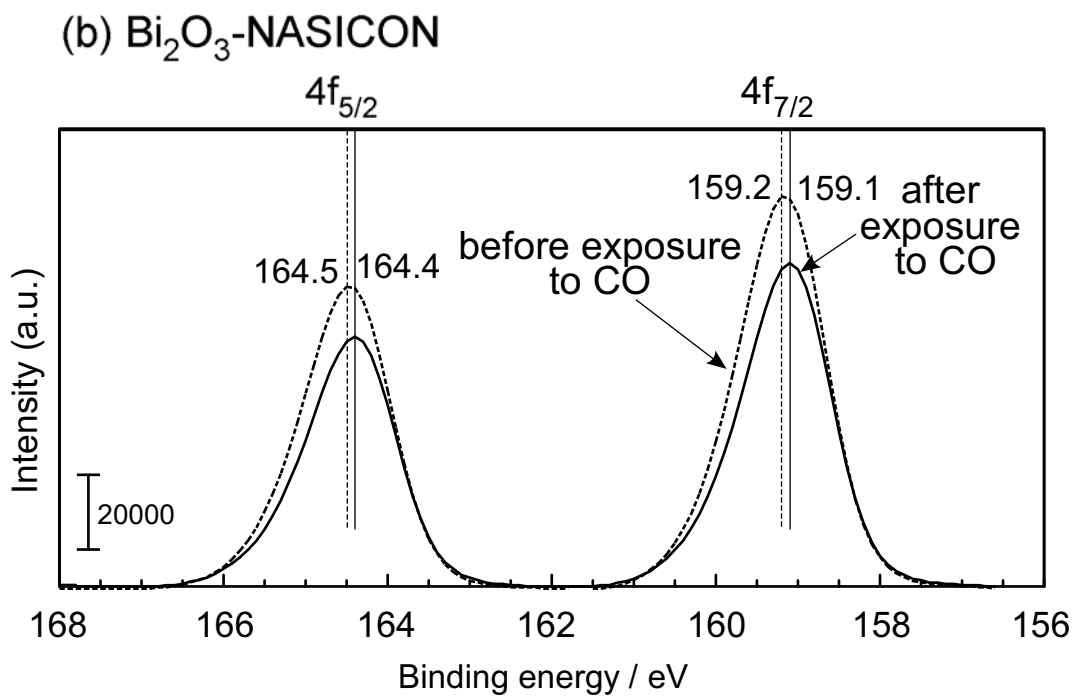
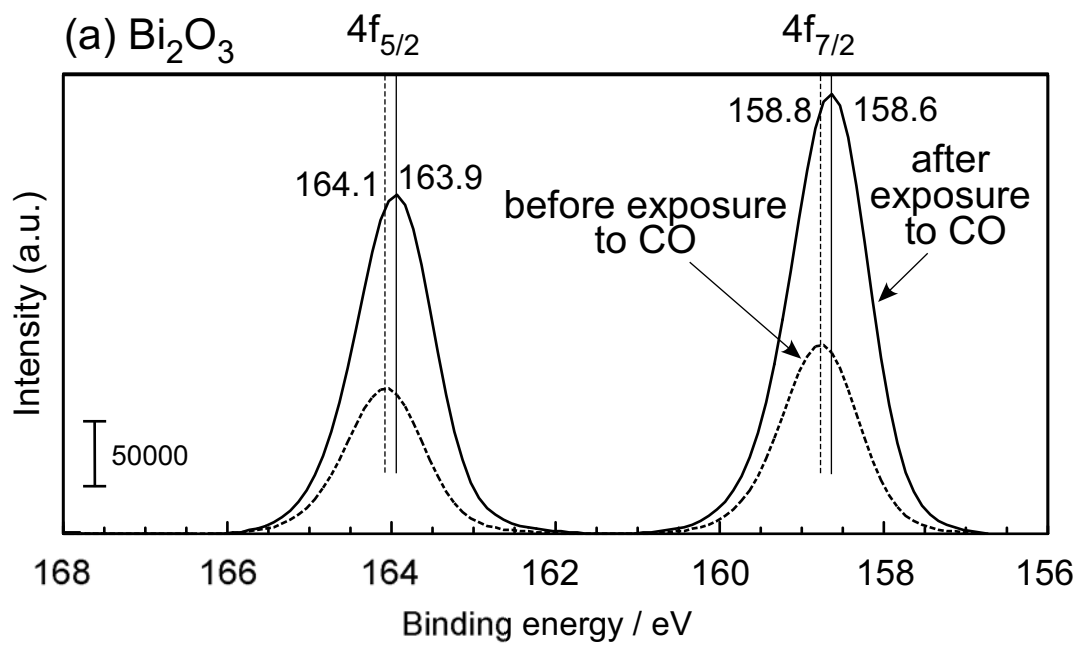


Fig. 4. Ueda et al.

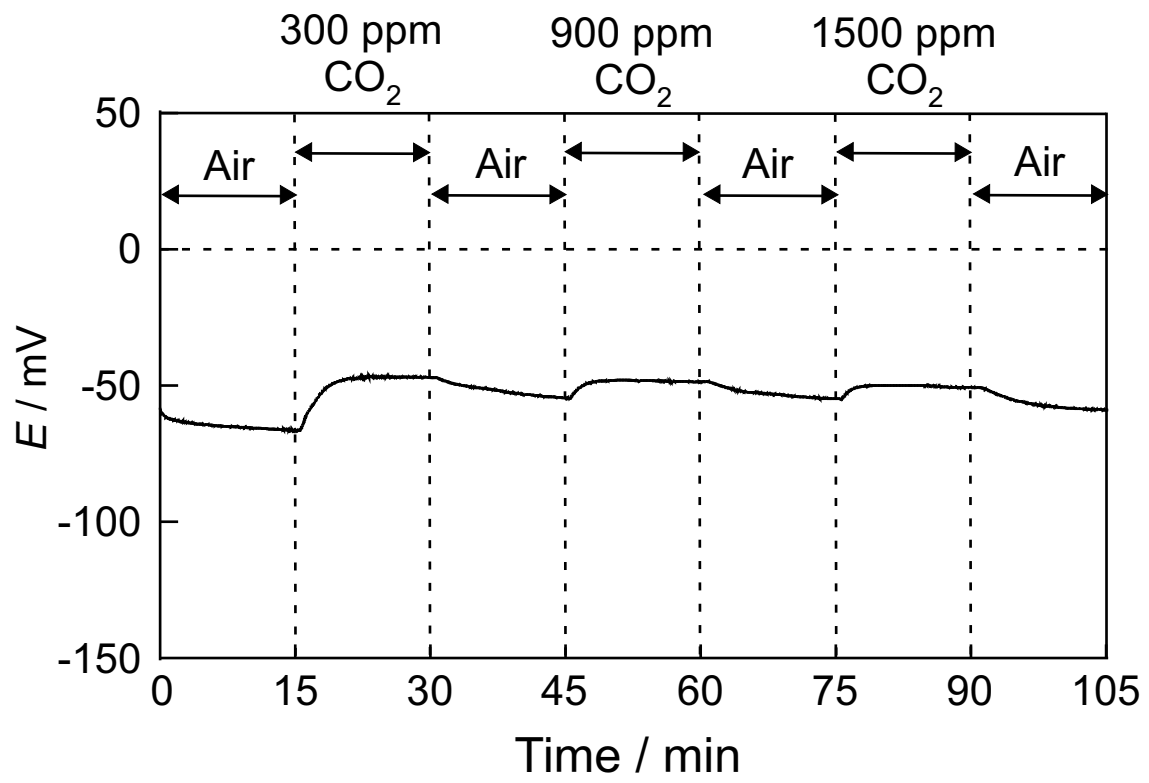


Fig. 5. Ueda et al.

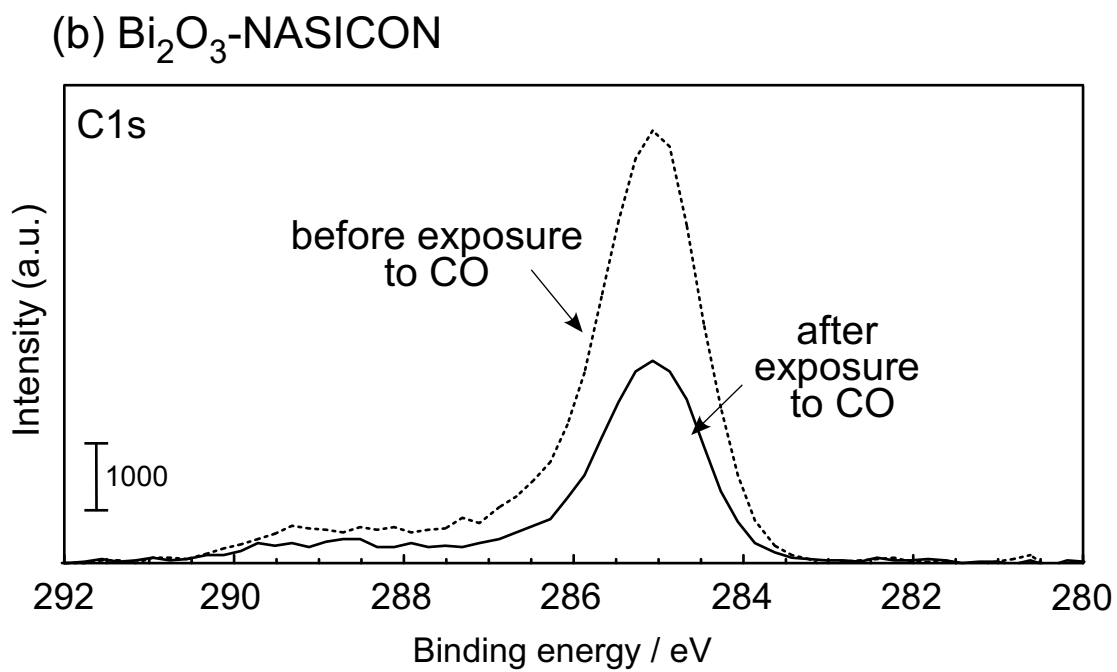
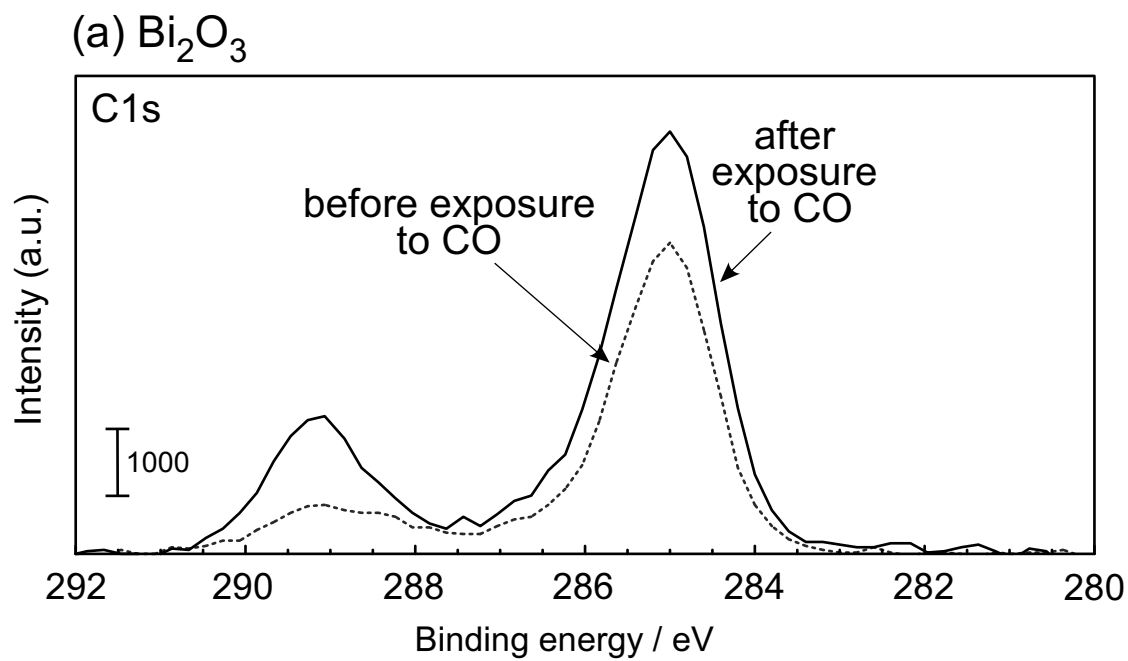


Fig. 6. Ueda et al.

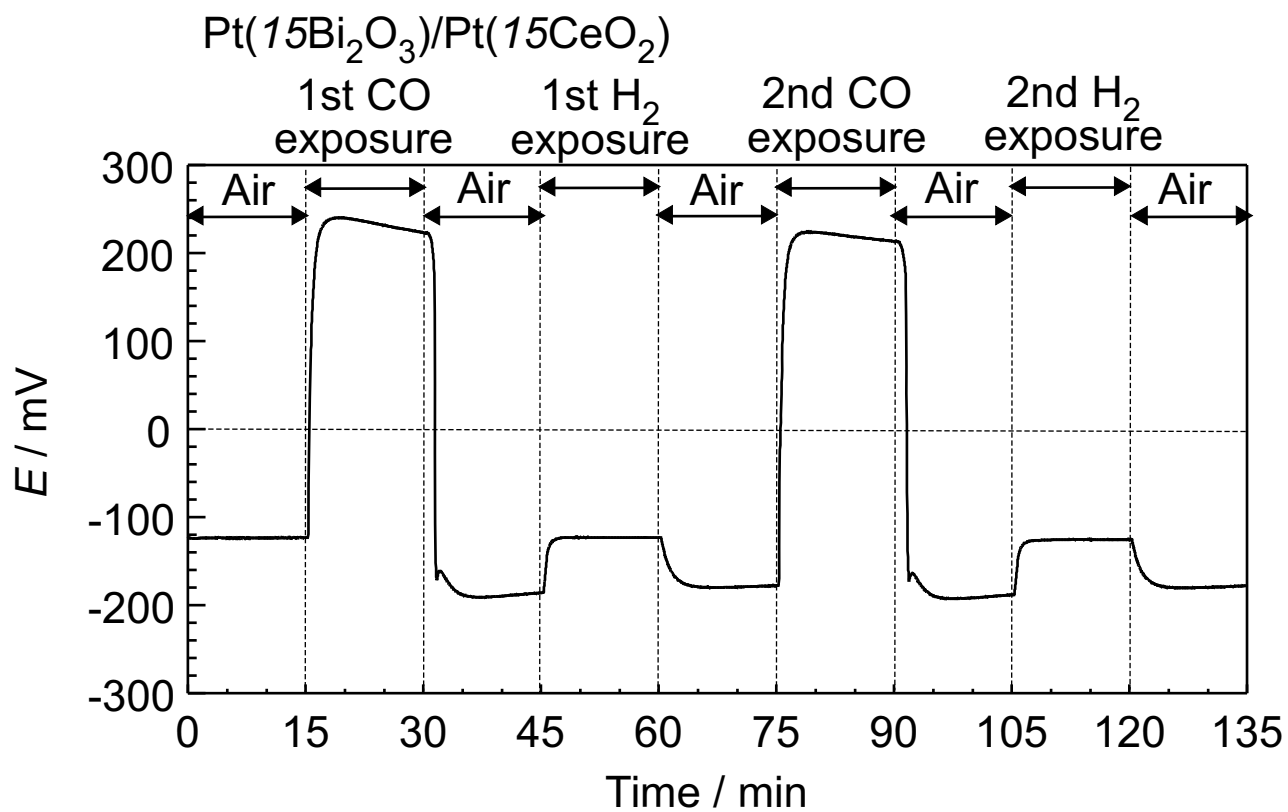


Fig. 7. Ueda et al.